Vol 11 No 1, January 2002
1009-1963/2002/11(01)/0044-06
Chinese Physics
© 2002 Chin. Phys. Soc.
and IOP Publishing Ltd

Three-dimensional modelling of the flow and heat transfer in a laminar non-transferred arc plasma torch*

Li He-Ping(李和平) and Chen Xi(陈 熙)†

Department of Engineering Mechanics, Tsinghua University, Beijing 100084, *China*

(Received 17 June 2001; revised manuscript received 10 September 2001)

By experimental observation we show that the plasma flow and heat transfer within a direct current (DC) non-transferred arc plasma torch always show appreciable three-dimensional (3D) peculiarity even when the geometrical construction of the torch and working gas admission and external electrical collection conditions are completely axisymmetrical. Previous two-dimensional (2D) modelling studies cannot predict the 3D peculiarity of the plasma torch. We have successfully performed 3D modelling, and in this paper we present the modelling results for the plasma flow and heat transfer characteristics in a laminar DC non-transferred arc argon plasma torch. The predicted arc-root location on the surface of the torch anode and arc voltage compare favourably with the corresponding experimental results.

Keywords: plasma torch, non-transferred arc, 3D modelling
PACC: 5230, 5280

1. Introduction

Direct current (DC) non-transferred arc plasma torches have been widely used in producing thermal plasma jets with both electron and heavy-particle temperatures around 10^4K. They have found various applications in industry and in laboratories, among which a few examples are atmospheric or low-pressure plasma spraying, thermal plasma waste treatment, plasma assisted chemical vapour deposition and plasma preparation of diamond films or ultra-fine powders.[1,2] In order to gain a better understanding of the physical processes occurring in the DC arc plasma torch and to optimize related parameters, much research (see, for example, Refs.[3]–[5] and references cited therein) has been carried out to model the plasma flow and heat transfer inside the plasma torch. The physical processes in an arc plasma torch are quite complex. The plasma flow and heat transfer are coupled with the electromagnetic field, and there is always a great temperature difference in the thermal plasma system. Thus, the temperature-dependent thermodynamic and transport properties of the plasma must be considered to vary over a wide range. Many other complicated factors may also be involved, such as the unsteady effects caused by arc-root fluctuation, the non-local thermodynamic equilibrium (non-LTE) effects near the electrodes or cold wall, the three-dimensional (3D) flow effects due to the local attachment of the arc at the anode surface, etc.[1,2] In order to simplify the problem and to save computer resources, usually LTE and optically thin plasma, steady and two-dimensional (2D) or axisymmetrical flow assumptions have been used in most previous modelling studies. Although these studies can give some useful information concerning the plasma torch characteristics and are often used to give the torch outlet velocity and temperature profiles for subsequent plasma jet modelling,[3,4] the 2D modelling approach is not quite satisfactory because it cannot fully describe the actual torch processes. For example, the 2D modelling in Ref.[5] concerning the DC non-transferred arc plasma torch, which is plotted in Fig.1 and has been used in our laboratory,[2] predicted an arc voltage for the turbulent regime much higher (by two or three times) than the measured value. Also, the predicted axial location of the arc-root attachment at the anode surface was much further downstream than that observed in experiments. It is believed that the main reason for such a great discrepancy is due to the intrinsic axisymmetric assumption of the 2D modelling. The axisymmetrical assumption necessarily leads to a circumferentially uniform arc attachment at the torch anode-nozzle, and thus all the oncoming cold working gas must be forcibly heated by the arc itself. The arc-root is consequently pushed by the gas

*Project supported by the National Natural Science Foundation of China (Grant Nos. 59836220 and 50176024).
†Author to whom correspondence should be addressed. E-mail: cx-dem@mail.tsinghua.edu.cn

flow to a location further downstream. Our experimental observation indicated that the arc root in the torch shown in Fig.1 always only partly attaches to the anode surface in the azimuthal direction. Hence most of the cold gas can flow around the arc (instead of passing through the arc), and the flow patterns inside the plasma torch must have 3D peculiarity. Using the so-called fictitious anode[4,5] in 2D modelling may improve the prediction of the arc voltage, but cannot predict the 3D flow and heat transfer characteristics of the plasma torch. As a novel approach, this paper employs 3D modelling to investigate the 3D flow and heat transfer inside the axisymmetrical DC non-transferred arc plasma torch shown in Fig.1 (hereafter referred to as simply the torch).

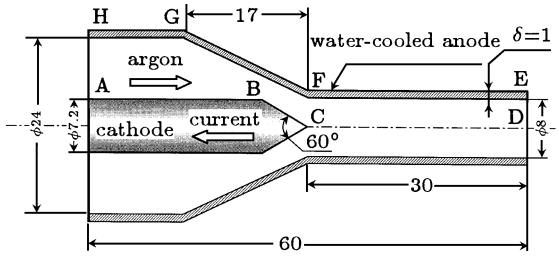


Fig.1. Schematic diagram of the DC non-transferred arc plasma torch under study.

A few papers have been published concerning 3D modelling of a gas-blown or magnetically deflected arc or a non-transferred arc plasma torch (see, for example, Refs.[6]–[10]). The common feature of these papers is that some asymmetrical external conditions are always introduced to ensure the 3D flow effects. For example, non-axisymmetrical geometrical construction was involved in Refs.[7]–[10], the applied magnetic field was considered in Refs.[6] and [7], the cross flow effects were studied in Ref.[9], whereas the working gas was admitted through three separate holes on the upstream side of the torch in Ref.[10]. However, for the torch under study, there are no external conditions to cause the 3D flow effects; namely, the torch is geometrically axisymmetrical, and no circumferential non-uniformity can be found in the working gas admission or in the electrical-cable collection. In this situation, the problem of how to model the 3D flow and heat transfer in the plasma torch is highly challenging. To our knowledge, so far no other researchers have considered this problem. The main difficulty is that one has to predict the 3D flow and heat transfer in the plasma torch without the help of any asymmetrical boundary conditions. Introducing any artificial 3D boundary conditions (e.g. a higher temperature is taken in a small region at the anode surface) may lead to unbelievable predictions, and thus is unacceptable. This difficulty has been successfully overcome in our recent study. Here we give the predicted results of the 3D flow and temperature fields in the torch and compare these with the results of the corresponding 2D modelling and with some experimental results. In order to avoid the complexity of modelling the turbulent plasma flow, the present study is restricted to the laminar argon plasma torch with a comparatively low flow rate of the working gas.

2. Modelling approach

In this paper, we consider mainly the 3D effects in the non-transferred arc plasma torch. Other assumptions are thus taken to be the same as those used in most previous studies,[2−5] including the steady flow, the optically thin and LTE plasma and the negligible gravity, viscous dissipation and pressure work.

Based on the foregoing assumptions, the continuity, momentum, energy and electrical potential equations in (r, θ, z) coordinates are[2]

$$\frac{1}{r}\frac{\partial}{\partial r}(r\rho v_r) + \frac{1}{r}\frac{\partial}{\partial \theta}(\rho v_\theta) + \frac{\partial}{\partial z}(\rho v_z) = 0, \qquad (1)$$

$$\begin{aligned}
&\rho\left(v_r\frac{\partial v_r}{\partial r} + \frac{v_\theta}{r}\frac{\partial v_r}{\partial \theta} + v_z\frac{\partial v_r}{\partial z}\right)\\
&= -\frac{\partial p}{\partial r} + \frac{\partial}{\partial r}\left(2\mu\frac{\partial v_r}{\partial r}\right)\\
&\quad + \frac{1}{r}\frac{\partial}{\partial \theta}\left[\mu\left(\frac{1}{r}\frac{\partial v_r}{\partial \theta} + \frac{\partial v_\theta}{\partial r} - \frac{v_\theta}{r}\right)\right]\\
&\quad + \frac{\partial}{\partial z}\left[\mu\left(\frac{\partial v_r}{\partial z} + \frac{\partial v_z}{\partial r}\right)\right]\\
&\quad + \frac{2\mu}{r}\left(\frac{\partial v_r}{\partial r} - \frac{1}{r}\frac{\partial v_\theta}{\partial \theta} - \frac{v_r}{r}\right) + \rho\frac{v_\theta^2}{r} + F_r, \qquad (2)
\end{aligned}$$

$$\begin{aligned}
&\rho\left(v_r\frac{\partial v_\theta}{\partial r} + \frac{v_\theta}{r}\frac{\partial v_\theta}{\partial \theta} + v_z\frac{\partial v_\theta}{\partial z}\right)\\
&= -\frac{1}{r}\frac{\partial p}{\partial \theta} + \frac{\partial}{\partial r}\left[\mu\left(\frac{\partial v_\theta}{\partial r} - \frac{v_\theta}{r} + \frac{1}{r}\frac{\partial v_r}{\partial \theta}\right)\right]\\
&\quad + \frac{1}{r}\frac{\partial}{\partial \theta}\left[2\mu\left(\frac{1}{r}\frac{\partial v_\theta}{\partial \theta} + \frac{v_r}{r}\right)\right]\\
&\quad + \frac{\partial}{\partial z}\left[\mu\left(\frac{\partial v_\theta}{\partial z} + \frac{1}{r}\frac{\partial v_z}{\partial \theta}\right)\right]\\
&\quad + \frac{2\mu}{r}\left(\frac{1}{r}\frac{\partial v_r}{\partial \theta} + \frac{\partial v_\theta}{\partial r} - \frac{v_\theta}{r}\right) - \rho\frac{v_r v_\theta}{r} + F_\theta, \qquad (3)
\end{aligned}$$

$$\begin{aligned}&\rho\left(v_r\frac{\partial v_z}{\partial r}+\frac{v_\theta}{r}\frac{\partial v_z}{\partial\theta}+v_z\frac{\partial v_z}{\partial z}\right)\\&=-\frac{\partial p}{\partial z}+\frac{1}{r}\frac{\partial}{\partial r}\left[\mu r\left(\frac{\partial v_z}{\partial r}+\frac{\partial v_r}{\partial z}\right)\right]\\&\quad+\frac{1}{r}\frac{\partial}{\partial\theta}\left[\mu\left(\frac{1}{r}\frac{\partial v_z}{\partial\theta}+\frac{\partial v_\theta}{\partial z}\right)\right]\\&\quad+\frac{\partial}{\partial z}\left(2\mu\frac{\partial v_z}{\partial z}\right)+F_z,\end{aligned}\tag{4}$$

$$\begin{aligned}&\rho c_p\left(v_r\frac{\partial T}{\partial r}+\frac{v_\theta}{r}\frac{\partial T}{\partial\theta}+v_z\frac{\partial T}{\partial z}\right)\\&=\frac{1}{r}\frac{\partial}{\partial r}\left(rk\frac{\partial T}{\partial r}\right)+\frac{1}{r^2}\frac{\partial}{\partial\theta}\left(k\frac{\partial T}{\partial\theta}\right)\\&\quad+\frac{\partial}{\partial z}\left(k\frac{\partial T}{\partial z}\right)-S_R+\frac{j_r^2+j_\theta^2+j_z^2}{\sigma}\\&\quad+\frac{5}{2}\frac{k_{\rm B}}{e}\left(j_r\frac{\partial T}{\partial r}+\frac{j_\theta}{r}\frac{\partial T}{\partial\theta}+j_z\frac{\partial T}{\partial z}\right),\end{aligned}\tag{5}$$

$$\frac{1}{r}\frac{\partial}{\partial r}\left(r\sigma\frac{\partial\phi}{\partial r}\right)+\frac{1}{r^2}\frac{\partial}{\partial\theta}\left(\sigma\frac{\partial\phi}{\partial\theta}\right)+\frac{\partial}{\partial z}\left(\sigma\frac{\partial\phi}{\partial z}\right)=0,\tag{6}$$

where ρ, μ, σ, c_p, k and S_R are the temperature-dependent argon density, viscosity, electric conductivity, specific heat at constant pressure, thermal conductivity and radiation power per unit volume of the plasma, respectively. T and ϕ are the gas temperature and electrical potential. v_r, v_θ and v_z are the components of the velocity vector in r-, θ- and z-directions, while j_r, j_θ and j_z are the r-, θ- and z-components of the current density vector $\boldsymbol{j}$, respectively. $k_{\rm B}$ is the Boltzmann constant, and e is the elementary charge. The current density vector can be related to the electrical potential by

$$\boldsymbol{j}=-\sigma\nabla\phi.\tag{7}$$

In Eqs.(2)–(4), F_r, F_θ and F_z are the r-, θ- and z-components of the Lorentz force $\boldsymbol{F}$, where

$$\boldsymbol{F}=\boldsymbol{j}\times\boldsymbol{B},\tag{8}$$

in which $\boldsymbol{B}$ is the magnetic induction vector.

Although the magnetic induction vector $\boldsymbol{B}$ can be calculated using the Biot–Savart law from the computed current density distribution in the iteration process, it is found to be a time-consuming task to calculate $\boldsymbol{B}$ in this way if a personal computer, such as a PII 400, is used. As an alternative approach, in this paper the magnetic vector potential ($\boldsymbol{A}$) equation[2]

$$\nabla^2\boldsymbol{A}=-\mu_0\boldsymbol{j}\tag{9}$$

is used to solve $\boldsymbol{A}$ and then the magnetic induction vector is calculated by using $\boldsymbol{B}=\nabla\times\boldsymbol{A}$. Here μ_0 is the magnetic permeability in free space.

The governing equations (continuity, momentum, energy, electrical potential and magnetic vector potential equations) were solved in the axisymmetrical computational domain formed by the revolution of the region ABCDEFGHA shown in Fig.1 around the torch axis. A special feature of this modelling study is that the arc cathode is excluded but the anode wall is included in the computational domain in order to predict more realistic inner surface temperatures of the water-cooled anode for the case with local arc attachment. A non-orthogonal boundary-conforming grid, non-staggered variable arrangement and SIMPLE algorithm are employed for the solution of the governing equations. Axisymmetrical boundary conditions are still used in the present modelling. Namely, at the torch inlet, the uniform axial velocity (v_z) profile, zero radial and tangent velocity components, zero electrical current density and room temperature are used. One-way boundary conditions ($\partial/\partial z=0$) are used at the torch exit. Averaged values of the physical quantities at the grid points in the mesh on the small circle nearest to the torch axis are taken as their values at the torch axis. The values of the magnetic vector potential along the outer boundaries are calculated by using the Biot–Savart law. The current density (assumed to be a Gaussian distribution as in Ref.[11]) and temperature distributions are given at the cathode tip. Room temperature, zero velocity components and zero electrical potential are adopted along the outer surface of the anode-nozzle. In this preliminary study, a 22 (r-direction)×11 (θ-direction, covering angle of $0-2\pi$)×32 (z-direction) mesh is employed. One may refer to Ref.[12] for a more detailed discussion.

3. Results and discussion

Typical modelling results are presented in Figs.2–5 for the case with an arc current of 200A and an argon flow rate of 0.35 STP m^3/h. Figure 2 shows the 3D modelling results for the temperature distributions within the plasma torch in two planes, which are perpendicular to each other and denoted by "$0-\pi$ plane" and "$\pi/2-3\pi/2$ plane". For comparison, the corresponding 2D modelling results are shown in Fig.3 for the isotherms within the same torch and with the same arc current, argon flow rate and boundary conditions, but using an additional axisymmetrical assumption. A comparison of the computed isotherms presented

in Fig.2 with those in Fig.3 shows that the 3D flow effect inside the plasma torch is quite obvious. The isotherms in the "$0-\pi$ plane" predicted by the 3D modelling are appreciably different from those in the "$\pi/2-3\pi/2$ plane", showing the 3D peculiarity of the heat transfer and fluid flow within the plasma torch. Figure 4 presents the 3D modelling results for the flow fields in the same two planes as in Fig.2, i.e. in the "$0-\pi$ plane" and "$\pi/2-3\pi/2$ plane". The 3D flow (non-axisymmetrical) peculiarity is also clearly seen in Fig.4.

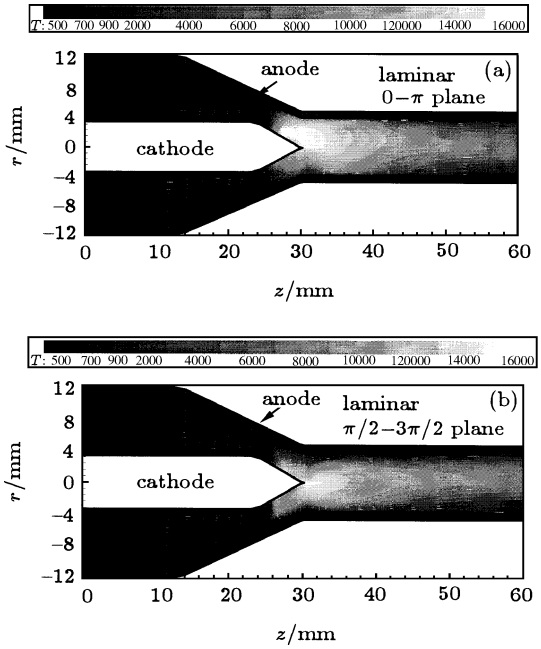


Fig.2. 3D modelling results for the temperature distributions within the plasma torch in two planes perpendicular to each other: (a) in the $0-\pi$ plane; (b) in the $\pi/2-3\pi/2$ plane. The arc current is 200A, and the argon flow rate is 0.35 STP m^3/h.

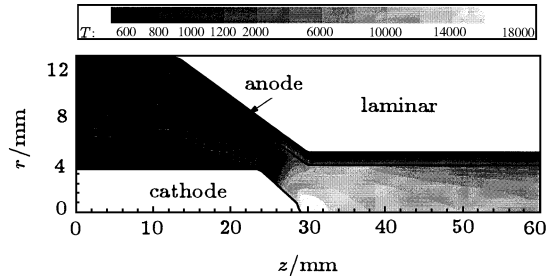


Fig.3. 2D modelling results for the temperature distribution within the plasma torch: arc current, 200A; argon flow rate, 0.35 STP m^3/h.

An additional comparison between the 3D and 2D modelling results is shown in Table 1, where T_{max} and U_{max} are the maximum temperature and axial velocity within the plasma torch, and T_{om} and U_{om} are the maximum values of the temperatures and axial velocities at the torch exit section, respectively. V_{cal} and V_{exp} are the calculated and experimentally measured arc voltages of the torch. It can be seen that there is a marked difference between in the predicted plasma torch characteristics of the 3D and 2D modelling approaches. The predicted value of the arc voltage of the present 3D modelling is higher than that of the 2D modelling, and the voltage predicted by the 3D modelling is closer to the measured value than that of the 2D modelling. In addition, the present 3D modelling predicts that the arc attachment region at the anode surface is near the intersection (z=30mm) of the conical part and the cylindrical part of the anode, and the arc attachment is not uniform in the azimuthal direction at the anode surface. Figure 5 shows the predicted distribution of the radial current density component along the inner surface of the water-cooled copper anode. A local high current density region at the inner surface of anode wall is seen clearly in Fig.5 due to the special feature of the local arc attachment. These predicted results are consistent with our experimental observation. Figure 6 shows a picture of the torch anode with an incrustation pattern at the outer surface after the arc plasma torch has been operated for tens of hours. The incrustation layer is always formed slowly in the high wall temperature region of the outer surface of the water-cooled copper anode during the torch opera-

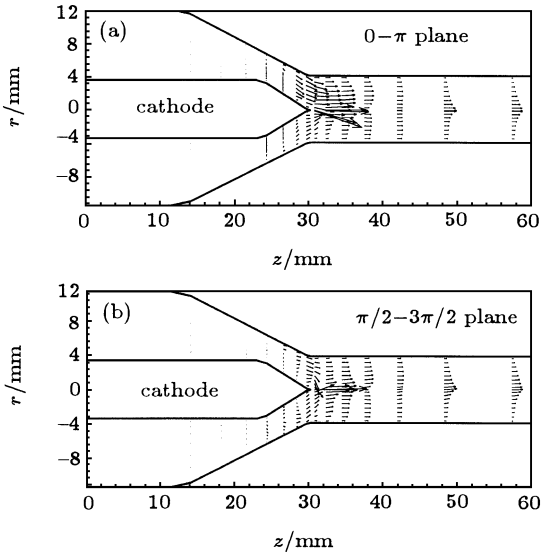


Fig.4. Predicted flow fields by the 3D modelling approach in two planes perpendicular to each other: (a) in the $0-\pi$ plane; (b) in the $\pi/2$–$3\pi/2$ plane. The arc current is 200A, and the argon flow rate is 0.35 STP m^3/h.

tion. When the thickness of the incrustation layer is

great enough, the incrustation layer may even break away from the anode surface. The high wall temperature region at the outer surface of the water-cooled anode should correspond to the location of the arc attachment at the inner surface of the anode. Figure 6 clearly demonstrates that the arc attachment at the anode surface is indeed circumferentially non-uniform, and the axial location of the arc attachment is near the intersection of the conical part and the cylindrical part of the anode. Thus, the arc attachment at the anode surface predicted by the present 3D modelling is very consistent with our experimental observation.

Table 1. Comparison between 3D and 2D modelling results concerning the torch characteristics. The measured value of the arc voltage is also given in the last column. The arc current is 200A and the argon flow rate is 0.35 STP m^3/h.

Case	T_{max}/K	U_{max}/(m/s)	T_{om}/K	U_{om}/(m/s)	V_{cal}/V	V_{exp}/V
2D	19969	253	10267	115	11.4	17.0
3D	20293	431	8815	76	13.9	

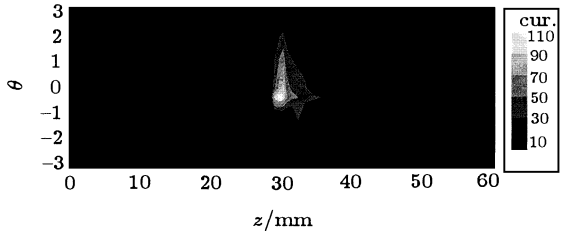


Fig.5. Predicted distribution of the radial current density component along the inner surface of the anode wall by 3D modelling (units: $\times 10^5 A/m^2$). The arc current is 200A, and the argon flow rate is 0.35 STP m^3/h.

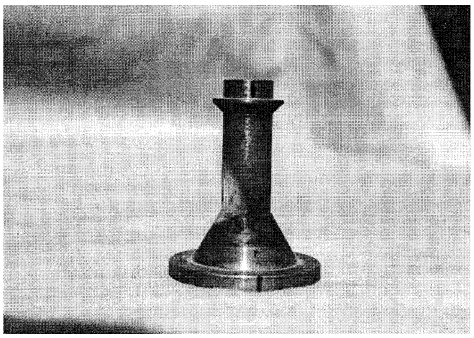


Fig.6. Photograph of the arc anode after tens of hours of operation, showing the incrustation pattern at the outer surface of the arc anode.

One may ask why the 3D flow and heat transfer can be predicted for the non-transferred plasma torch with completely axisymmetrical geometrical construction and axisymmetrical boundary conditions. The reason seems to be as follows. Even for the initial condition with a circumferentially uniform arc attachment at the anode surface, small random perturbations (e.g. produced in the numerical iteration) may result in the formation of a circumferentially non-uniform arc attachment. For example, in the iteration process of the numerical computation, if the local gas temperature at some angular location (e.g. $\theta = 0$) near the inner surface of the arc anode is somewhat higher than that at other angular locations, the electrical current density at this special location will increase due to the increase of gas electrical conductivity. Such a local higher current density will cause the enhancement of the already higher temperature at this special location. Since the total arc current is fixed, the enhancement of the current density at some location on the anode surface must cause the decrease of the current densities at other locations. As a result, this positive-feedback process in the iteration process will result in the formation of the local arc attachment in a certain azimuthal position on the inner surface of the anode wall. Of course, the precise axial location of the arc-root attachment is determined by the solution of the governing equations with associated boundary conditions. The formation of the local arc attachment must lead to the characteristics of 3D flow and heat transfer within the plasma torch, as shown in Figs.2, 4 and 5. It is noted that although Figs.2 and 5 show that the arc attachment appears near the angular location θ=0, actually the arc root location is circumferentially arbitrary since the actual angular position at the arc anode corresponding to θ=0 is arbitrarily chosen in the computation. It is expected that the local arc attachment at the anode surface will result in local thermal deformation, or even in slight damage of the anode surface. As soon as this local region with the mentioned "drawbacks" is formed at the inner surface of the plasma torch anode during the torch operation, the arc will prefer to attach there in subsequent operations, resulting in the incrustation pattern shown in Fig.6 after tens of hours of operation. It is quite possible that the axisymmetrical flow regime within the DC non-transferred arc plasma torch is inherently

unstable. The assessment of this possibility would be an interesting topic of subsequent theoretical studies.

4. Conclusions

DC non-transferred arc plasma torches often assume appreciable 3D flow and heat transfer peculiarity, even with completely axisymmetrical conditions in their geometrical configuration, working gas admission and electrical collection. The problem of how to model the 3D flow and heat transfer for this situation is challenging and long unresolved, due to the difficulty encountered in determining the unknown arc attachment location. This difficulty has been overcome for the first time in this study, and the 3D laminar flow and heat transfer characteristics in the DC non-transferred arc argon plasma torch have been successfully predicted. It is shown that the 3D modelling, in comparison with its 2D counterpart, can predict more realistic arc root location and arc voltage.

References

[1] Fauchais P and Vardelle A 2000 *Plasma Phys. Control. Fusion* **42B** B365

[2] Chen X 1993 *Heat Transfer and Fluid Flow under High-Temperature Ionized Gas Conditions* (Beijing: Science Press) chaps 1, 3, 6 (in Chinese)

[3] Westhoff R and Szekely J 1991 *J. Appl. Phys.* **70** 3455

[4] Bauchire J M, Gonzalez J J and Gleizes A 1997 *Plasma Chem. Plasma Process* **17** 409

[5] Han P 1999 Numerical and experimental studies on the characteristics of DC arc plasma torches and jets *PhD Thesis* Department of Engineering Mechanics, Tsinghua University (in Chinese)

[6] Kaddani A, Zahrai S, Delalondre C and Simonin O 1995 *J. Phys. D: Appl. Phys.* **28** 2294

[7] Speckhofer G and Schmidt H-P 1996 *IEEE Trans. Plasma Sci.* **24** 1239

[8] Schlitz L Z, Garimella S V and Chan S H 1999 *J. Appl. Phys.* **85** 2547

[9] Kelkar M and Heberlein J 2000 *J. Phys. D: Appl. Phys.* **33** 2172

[10] Freton P, Gonzalez J J and Gleizes A 2000 *J. Phys. D: Appl. Phys.* **33** 2442

[11] Hsu K C, Etemadi K and Pfender E 1983 *J. Appl. Phys.* **54** 1293

[12] Li H P 2001 Studies of heat transfer and fluid flow in a DC arc plasma torch and plasma jet *PhD Thesis* Department of Engineering Mechanics, Tsinghua University (in Chinese)